Jansen, M., Lissenberg, J., Klaver, M., de Graaff, S., Koornneef, J., Smeets, R., MacLeod, C., & Davies, G. (2018). Isotopic variation in Semail Ophiolite lower crust reveals crustal-level melt aggregation. *Geochemical Perspectives Letters*, *8*, 37-42. https://doi.org/10.7185/geochemlet.1827

Geochemical Perspectives Letters

Isotopic variation in Semail Ophiolite lower crust reveals crustal-level melt aggregation

M.N. Jansen[1,2*], C.J. Lissenberg[1], M. Klaver[3], S.J. de Graaff[2,4], J.M. Koornneef[2], R.J. Smeets[2], C.J. MacLeod[1], G.R. Davies[2]

doi: 10.7185/geochemlet.1827

Abstract

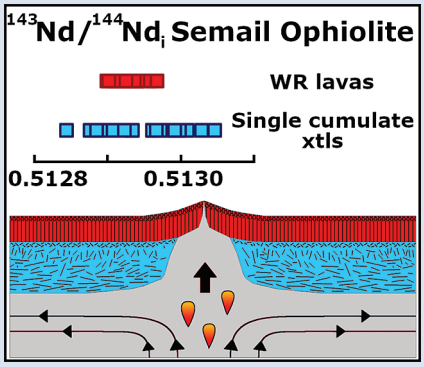

The scale and magnitude of compositional heterogeneity in the mantle has important implications for the understanding of the evolution of Earth. Heterogeneity of the upper mantle is often evaluated based on mid-ocean ridge basalt compositions, despite their homogenisation prior to eruption. In this study we present Nd and Sr isotope data obtained by micro-drilling single plagioclase and clinopyroxene crystals in gabbroic cumulates of the Semail Ophiolite (Oman) and show that mantle source variability is better preserved in the lower crust than in the extrusive suite. Analysis of sub-nanogram quantities of Nd in plagioclase revealed a range in $^{143}Nd/^{144}Nd_i$ in the Wadi Abyad crustal section that is three times greater than recorded in the extrusive suite. The isotopic variability is preserved in plagioclase, whereas clinopyroxene is isotopically homogeneous. These data imply that the mantle is heterogeneous on the scale of melt extraction, and that a significant proportion of homogenisation of erupted melts occurs in the oceanic crust, not the mantle.

Received 15 April 2018 | Accepted 10 October 2018 | Published 5 November 2018

Introduction

Planetary differentiation and plate tectonics have led to marked compositional heterogeneity in Earth's mantle. Quantification of the scale and magnitude of mantle heterogeneity has important implications for the understanding of these processes and is one of the major challenges in geochemistry. Because the mantle cannot be sampled directly, this problem remains unresolved. Mid-ocean ridge basalts (MORB) are the most voluminous magmatic rocks on Earth, continually resurfacing two-thirds of the planet on an approximately 200 Myr timescale. They form through decompression melting of the upper mantle and typically undergo partial crystallisation in crustal magma chambers before being erupted onto the seafloor (*e.g.*, Klein and Langmuir, 1987). Long-lived radiogenic isotopes are insensitive to crystallisation processes and are robust mantle source tracers. Many studies have therefore focused on the isotopic composition of MORB to assess along-ridge mantle heterogeneity (*e.g.*, Zindler *et al.*, 1979). Magmatic processes at mid-ocean ridges, however, act to homogenise discrete magma batches (*e.g.*, Rubin and Sinton, 2007), thus obscuring variability at the scale of melt extraction. Homogenisation of isotopic variability is particularly common at fast-spreading ridges, where higher melt production enhances magma mixing and reduces mantle-related variation in MORB compositions (Rubin and Sinton, 2007). Melt batch-scale heterogeneity is partially preserved in phenocrysts and their melt inclusions, which are believed to record unaggregated melt compositions (*e.g.*, Lange *et al.*, 2013). This suggests that lower crustal cumulates potentially record a greater isotopic variability than their extrusive counterparts.

Explicit consideration for the scale of sampling is essential for a full understanding of the lower oceanic crust due to the presence of significant compositional heterogeneity at scales ranging from millimetres to hundreds of metres (*e.g.*, Lissenberg *et al.*, 2013; Coogan, 2014). Whole rock geochemical analyses cannot resolve sample- or crystal-scale variations. Isotopic heterogeneity within individual minerals is to be expected if crystal growth spans replenishment and magma mixing episodes (Davidson and Tepley, 1997; Lange *et al.*, 2013). Furthermore, whole rock isotopic data may mask heterogeneity if overgrowth on cumulus minerals and/or intercumulus minerals crystallised from isotopically distinct migrating interstitial melts (Yang *et al.*, 2013).

1. School of Earth and Ocean Sciences, Cardiff University, Cardiff, United Kingdom
2. Faculty of Science, Vrije Universiteit, Amsterdam, the Netherlands
3. School of Earth Sciences, University of Bristol, Wills Memorial Building, Queens Road, Bristol BS8 1RJ, United Kingdom
4. Department of Analytical and Environmental Geochemistry, Vrije Universiteit Brussel, Brussels, Belgium
* Corresponding author (e-mail: JansenMN@cardiff.ac.uk)

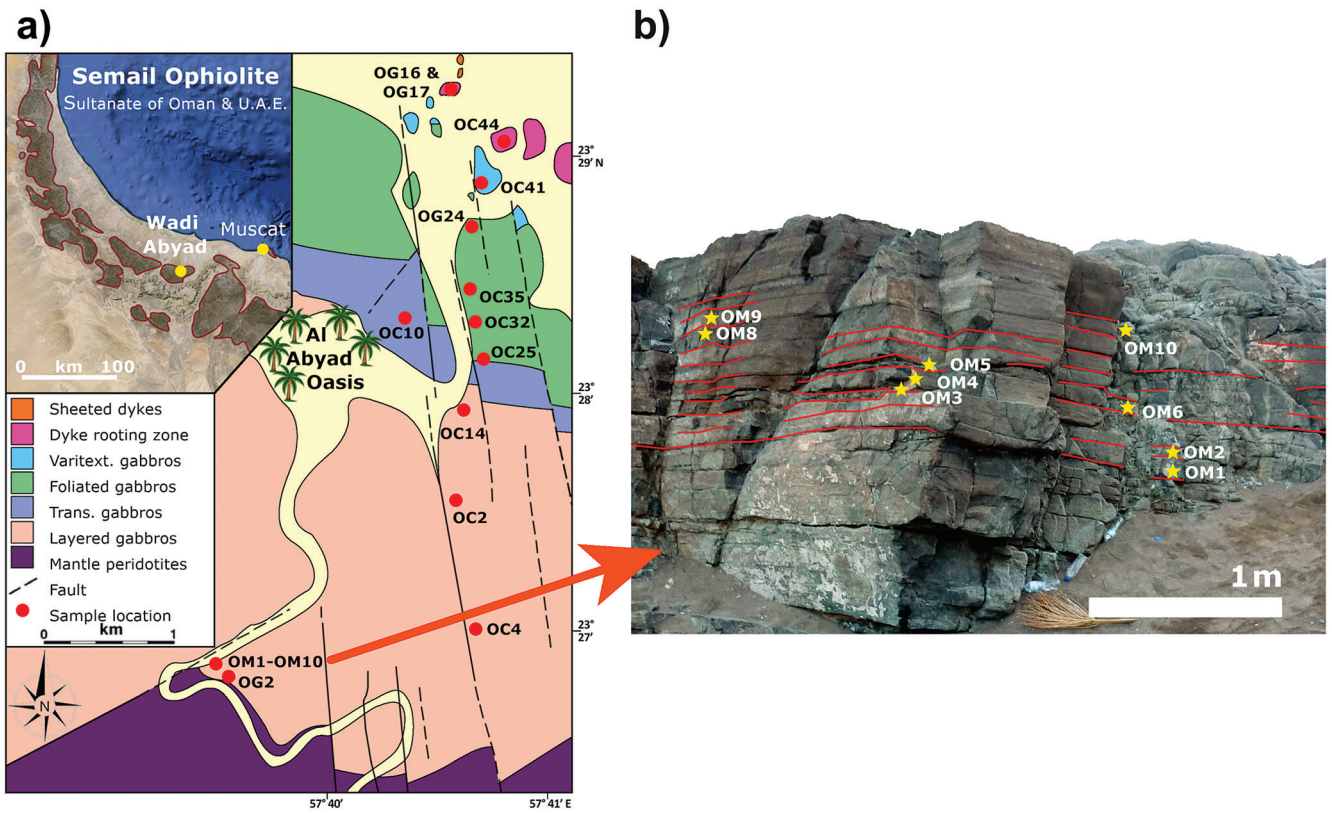

Figure 1 **(a)** Geological map of the lower crustal section at Wadi Abyad, in the Semail Ophiolite, Oman, with sample locations indicated (after MacLeod and Yaouancq, 2000; sample names were shortened by omitting the numerals '95' preceding the letters 'OC' and 'OG' and '14' preceding 'OM'). **(b)** An outcrop at the base of the layered gabbros was sampled at ~15 cm intervals (one sample per modal layer).

Due to its inaccessibility, oceanic crust is often studied using on-land analogues such as the 96 Ma Semail Ophiolite in Oman and the UAE (Nicolas, 1989; Rioux *et al.*, 2013). Although the Semail Ophiolite may have formed in a subduction-related setting (MacLeod *et al.*, 2013), its mode of formation and isotopic signature is comparable to MORB (Godard *et al.*, 2006) and therefore an ideal location for this study. A micro-sampling technique for plagioclase and clinopyroxene crystals allowed isotopic analyses of single mineral grains for which the textural context and geochemical composition were known and avoided averaging isotopic variations within a sample.

Geological Setting and Methods

The Semail Ophiolite lower crust at Wadi Abyad consists of a ~1700 m thick sequence of modally layered gabbros, overlain by non-layered, steeply-foliated gabbros (~650 m) and ~150 m of varitextured gabbros and a 'dyke rooting zone' transition into the base of a sheeted dyke complex (MacLeod and Yaouancq, 2000). Thirteen gabbros and olivine-gabbros spanning the entire lower crustal stratigraphy were sampled at an average interval of ~200 m, complemented with nine sampled modal layers (~15 cm thick) from a single outcrop near the base of the layered gabbros (Fig. 1). Major and trace element data collected from thick sections by EMP and LA-ICPMS (Supplementary Information, Table S-4e) were combined with EDS-SEM major element mapping of polished rock slabs to select domains most suitable for micro-sampling in the latter. Single crystal isotopic analyses (Nd and Sr in plagioclase; Nd in clinopyroxene) were performed on material obtained by micro-drilling individual crystals. The amount of Nd recovered ranged between ~1-5 ng in clinopyroxene and ~0.1-0.5 ng in plagioclase, while ~500 ng Sr was obtained from plagioclase. Plagioclase samples were spiked with a ^{149}Sm-^{150}Nd mixed-spike prior to digestion for Sm/Nd isotope dilution analysis. Chemical separation for Sr, Nd and Sm was performed using standard ion exchange techniques and samples were measured on a Thermo Scientific Triton *Plus* thermal ionisation mass spectrometer (TIMS), using 10^{13} Ω amplifiers for the measurement of Sm (50-250 pg) and Nd in the plagioclase samples. Isotope ratios were age-corrected to 96 Ma (subscript "i"; Rioux *et al.*, 2013). The reproducibility (2 SD) of ^{143}Nd/^{144}Nd for BCR-2 reference material is 161 ppm for aliquots of 0.15-0.34 ng Nd and 82 ppm for aliquots of 1.9-2.6 ng Nd. A detailed description of the methods and results for internal and external standards is provided in the Supplementary Information.

Results

Plagioclase and clinopyroxene crystals have ^{143}Nd/^{144}Nd$_i$ typical of MORB, with values ranging from 0.512844 to 0.513046 (Figs. 2 and 3, Supplementary Information, Table S-4a-d). Clinopyroxene samples reveal an almost uniform Nd isotope composition, with a range of 225 ppm and only two samples, from the foliated gabbros and dyke rooting zone, are outside error (by 10 ppm); the ppm notation here indicating the range relative to the average ^{143}Nd/^{144}Nd$_i$ of the dataset (0.512936).

Plagioclase samples display a greater range in Nd isotope composition, 395 ppm, with the lowest values outside error of the highest values by up to 88 ppm (Fig. 2). This range is well in excess of the variation found in the extrusive suite of the entire Semail Ophiolite (whole rock; 134 ppm). It is also significantly larger than existing whole rock and mineral separate data for the lower crust (123 ppm). It is, however, comparable to the range found in gabbroic cumulates in the Maqsad mantle harzburgites (whole rock; 414 ppm), which are interpreted to be individual melt batches within a fossil mantle diapir (Benoit *et al.*, 1996; Fig. 4, all data sources in figure caption).

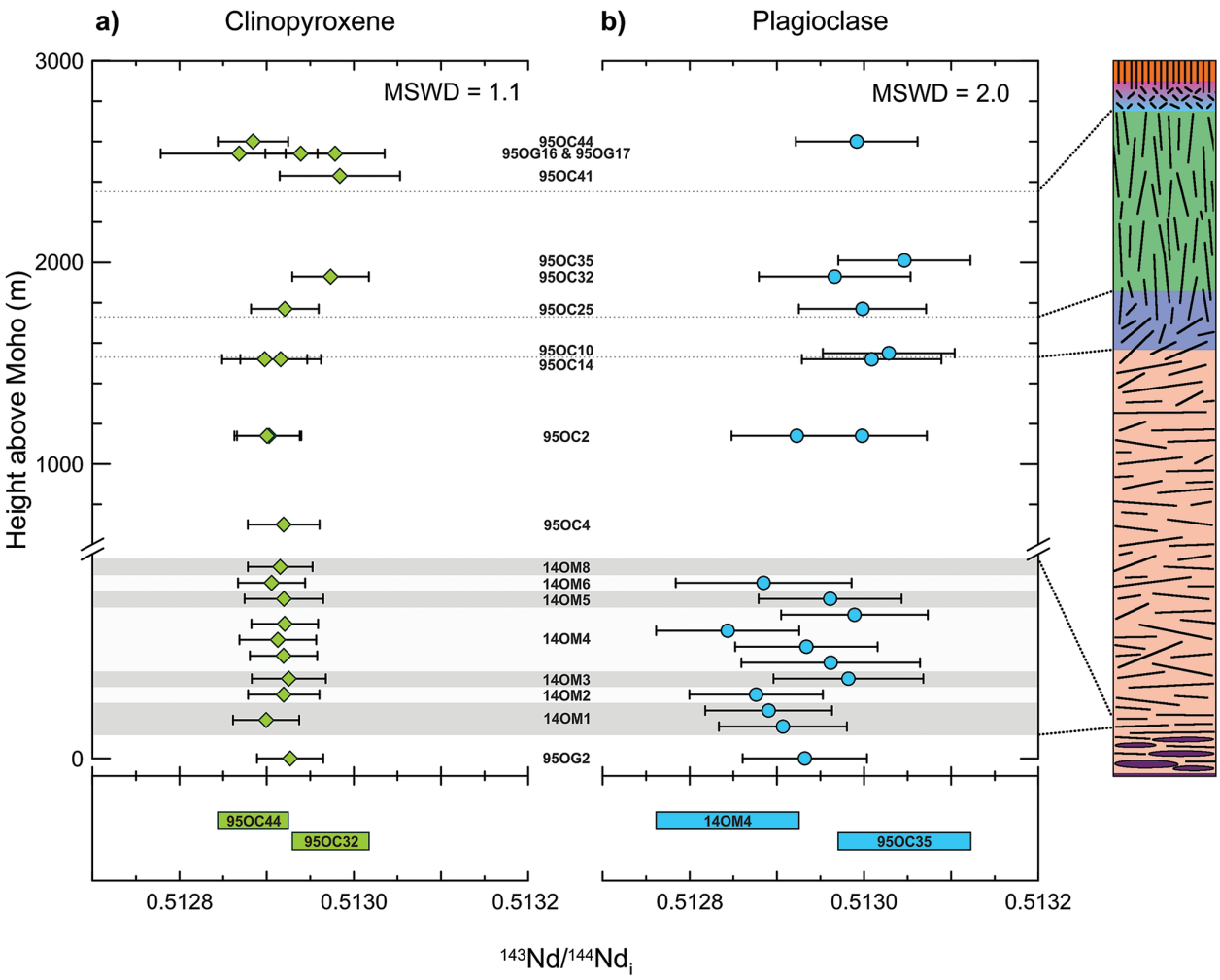

Figure 2 Age-corrected $^{143}Nd/^{144}Nd_i$ of **(a)** single clinopyroxene and **(b)** plagioclase crystals in the Abyad section. Clinopyroxene has a near uniform composition whereas plagioclase shows variability outside analytical uncertainty. Grey and white alternating bars at the base of the section indicate the individual modal layers of the sampled layered gabbro outcrop (not to scale). Coloured bars at the bottom of the figure represent the uncertainty for the two most extreme samples.

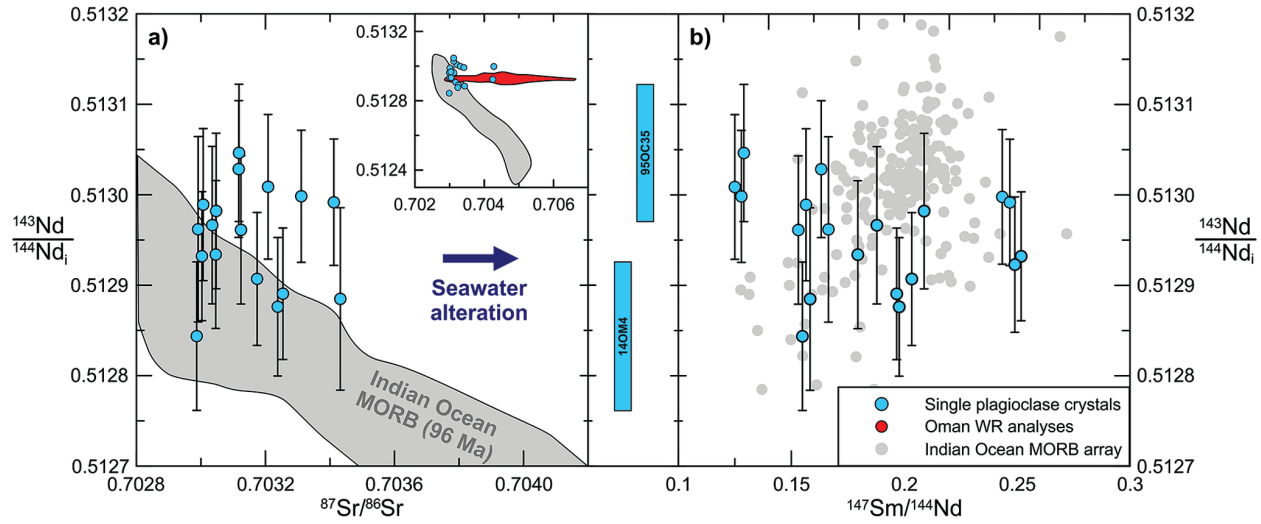

Figure 3 **(a)** Age-corrected $^{143}Nd/^{144}Nd_i$ and $^{87}Sr/^{86}Sr$ compositions of plagioclase samples. Indian Ocean MORB data from the PetDB database and age-corrected to 96 Ma using model Sm/Nd and Rb/Sr ratios for depleted MORB mantle (Workman and Hart, 2005). The ranges of whole rock age-corrected Sr and Nd isotope analyses of the plutonic and extrusive series of the Semail Ophiolite are shown in the inset (McCulloch *et al.*, 1980; Godard *et al.*, 2006; Rioux *et al.*, 2012, 2013; de Graaff, 2016). **(b)** Age-corrected $^{143}Nd/^{144}Nd_i$ and $^{147}Sm/^{144}Nd$ ratios show no correlation, whereas the present day Indian Ocean MORB array, shown for comparison, displays a broad positive correlation. Coloured bars in the centre panel represent the uncertainty in $^{143}Nd/^{144}Nd_i$ for the two most extreme samples.

The plagioclase Nd data (n = 19) yield a mean square weighted deviation (MSWD = 2.0) that is significantly greater than the critical value (1.7; following Wendt and Carl, 1991; see Supplementary Information), meaning that the probability that the data form a single, normally distributed population is <5 %. We therefore argue that the observed $^{143}Nd/^{144}Nd_i$ heterogeneity in plagioclase is statistically significant and represents a primary feature. The clinopyroxene data (n = 22) show an MSWD that is smaller than the critical MSWD (1.1 *versus* 1.6, respectively), implying that the clinopyroxene data constitute a statistically homogeneous population at the current level of precision.

There is no discernible stratigraphic trend in plagioclase isotopic composition and the samples record a relatively large range in $^{147}Sm/^{144}Nd$ ratios (0.13-0.25) that does not correlate with $^{143}Nd/^{144}Nd_i$ (Fig. 3). With the exception of two samples, Nd and Sr isotope ratios in plagioclase crystals are closer to the MORB array than whole rock isotopic analyses (red field in Fig. 3). It is difficult to interpret the variability of strontium isotopes in plagioclase purely in terms of mantle source as seawater alteration is known to elevate $^{87}Sr/^{86}Sr$ without affecting $^{143}Nd/^{144}Nd$ (McCulloch *et al.*, 1980). The limited range observed in the micro-drilled $^{87}Sr/^{86}Sr$ compositions potentially records less extensive seawater alteration but we cannot disentangle minor alteration from source heterogeneity.

Discussion

Our data represent the first micro-drilled Nd isotope mineral analyses for lower ocean crustal rocks and provide constraints on both ocean crustal and mantle processes. Compared to previous whole rock analyses of plutonic rocks, single plagioclase crystals record a larger Nd isotope variability and are thus much more suitable for studying the full extent of isotopic variability in the lower oceanic crust. The similarity of the observed Nd isotope range in plagioclase to the gabbros from the Maqsad diapir (Fig. 4), taken to represent individual melt batches in upwelling mantle (Benoit *et al.*, 1996), suggests that the lower crust preserves the heterogeneity of melt batches at a mineral scale. This implies that the upper mantle is compositionally heterogeneous at the scale of melt extraction (*e.g.*, Lange *et al.*, 2013), and that the melt extraction process did not fully homogenise melts. The isotopic variability in whole rock analyses of the overlying dykes and lavas, representing fully aggregated and erupted melts, is limited compared to plagioclase in the lower crust (Fig. 4) and indicates that the substantial mixing and homogenisation required to produce MORB takes place in the crust. Previous comparisons of upper crustal basalts to whole rock analyses of plutonic rocks led to a substantially different conclusion as illustrated in Figure 4 (*e.g.*, Coogan, 2014). The whole rock data alone suggest the upper

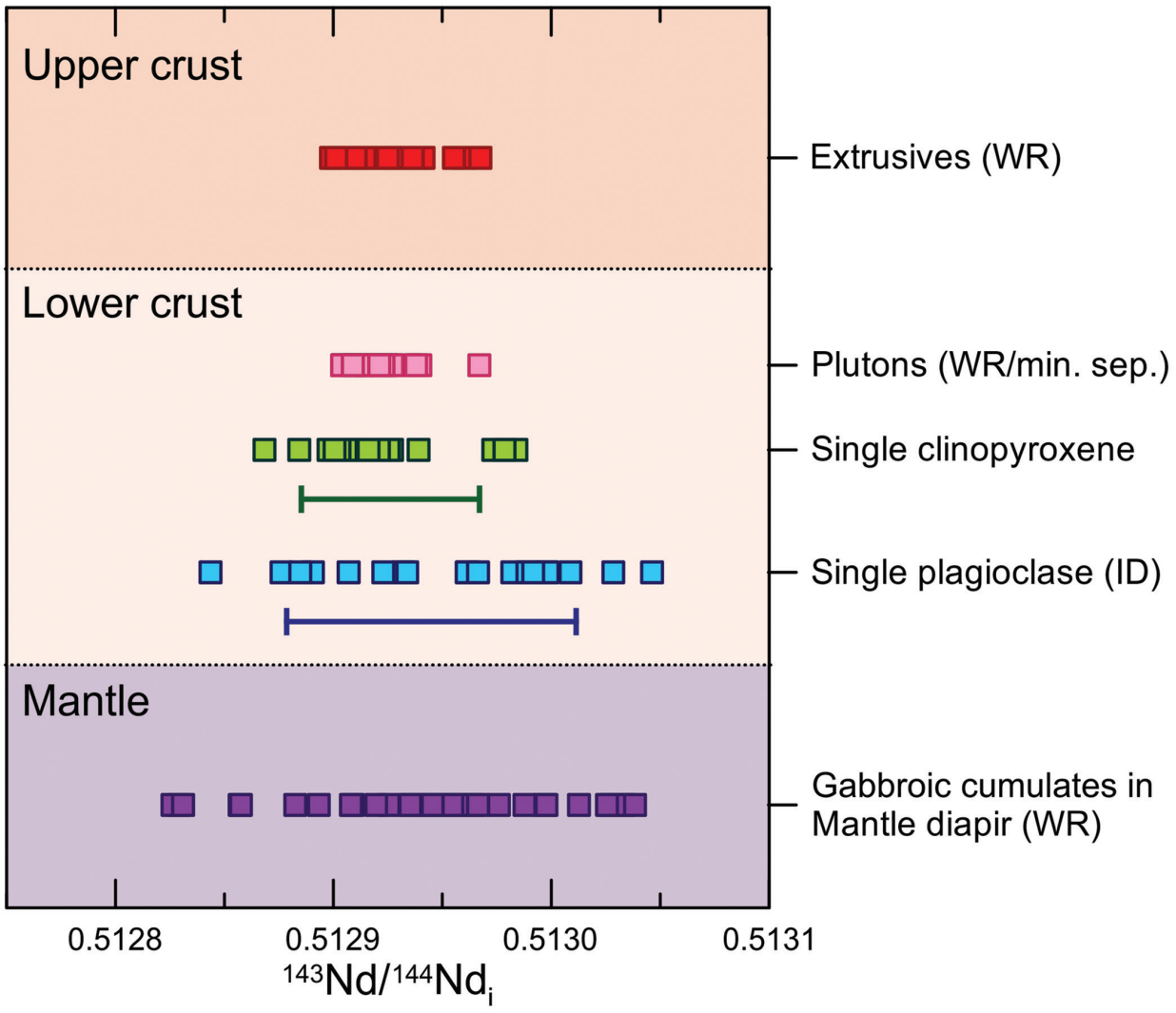

Figure 4 Comparison of the ranges in Nd isotopes found in this study with previous results of the Semail Ophiolite (McCulloch *et al.*, 1980; Benoit *et al.*, 1996; Godard *et al.*, 2006; Rioux *et al.*, 2012, 2013; de Graaff, 2016). Range for repeated analyses of BCR-2 reference material is indicated by the green (1.9-2.6 ng Nd) and blue (0.15-0.34 ng Nd) bars (displayed at an arbitrary position on the x-axis).

and lower crust formed from melts that were homogenised to similar extents. Our findings also contrast with Koga *et al*. (2001) who concluded that trace element variability in the Moho transition zone in the Semail Ophiolite is comparable to that in the upper crustal sheeted dyke complex and lavas and that mixing must have taken place predominantly in the mantle.

This study demonstrates that the approach of using mineral trace element ratios alone to study source compositions can be problematic. We find that plagioclase Sm/Nd does not correlate with $^{143}Nd/^{144}Nd_i$ (the time integrated Sm/Nd), whereas a positive correlation would be expected if Sm/Nd is inherited from a mantle source (Fig. 3). Several other processes can affect Sm/Nd, such as degree of mantle melting, fractional crystallisation, melt replenishment (O'Neill and Jenner, 2012), melt-rock reactions (Lissenberg and MacLeod, 2016) and variable partition coefficients due to changes in pressure, An %, pH_2O and melt composition (Bédard, 2006). Hence, it is difficult to interpret a source signature from plagioclase trace element compositions. Since Nd isotope ratios are not fractionated by these processes, they are uniquely suited for investigating sources of mantle derived melt.

The contrast in $^{143}Nd/^{144}Nd_i$ variability between clinopyroxene (homogeneous) and plagioclase (heterogeneous) can have multiple causes. The first is sub-solidus diffusion of REE. This unlikely to be responsible for homogenisation, however, since Nd diffusion coefficients of clinopyroxene are two orders of magnitude lower than plagioclase (van Orman *et al*., 2001; Cherniak, 2003) and modelling shows that diffusion would primarily affect plagioclase rather than clinopyroxene for conditions prevalent in the lower oceanic crust (Coogan and O'Hara, 2015).

The second is a crystallisation sequence of plagioclase before clinopyroxene during progressive magma mixing and associated homogenisation. Textures of Wadi Abyad gabbros are granular to intergranular, with an apparent olivine -> plagioclase -> clinopyroxene crystallisation sequence. The absence of troctolites in the section, however, may indicate a near simultaneous saturation of plagioclase and clinopyroxene (Thomas, 2003). Furthermore, moderate textural re-equilibration during slow cooling may obscure primary textures and make it difficult to distinguish co-crystallisation from sequential crystallisation (MacLeod and Yaouancq, 2000).

Finally, reactive porous flow of interstitial melts may be responsible for isotopic homogenisation in clinopyroxene. Migration of late stage melts by porous flow is pervasive throughout the entire lower crust (Lissenberg *et al*., 2013; Lissenberg and MacLeod, 2016). Clinopyroxene and plagioclase in gabbros at Wadi Abyad show features that have been ascribed to reactive porous flow, including an up-section increase in enrichment and fractionation of elements proportional to their incompatibility (*e.g.*, La/Nd and Ce/Y) and trace element disequilibrium between coexisting plagioclase and clinopyroxene (Lissenberg and MacLeod, 2016). If the migrating interstitial melts are isotopically homogeneous, as seems likely, melt-crystal reaction can conceivably homogenise isotopic variation in the lower crust. It is currently unclear, however, whether clinopyroxene is more sensitive to melt-rock reactions than plagioclase, as would be implied by the data: further work on this subject is required.

This work demonstrates that isotopic analysis of single grains in plutonic rocks has great potential to study the scale of mantle heterogeneity and the nature of crustal processes. By establishing that greater variability exists in the lower crust than in the erupted lavas of the Semail Ophiolite, we have shown that isotopic studies of whole rock MORB mask the full scale and extent of compositional heterogeneity of the mantle source. Micro-sampling successfully avoids interstitial grains and domains most affected by alteration (*i.e.* crystal rims) and, with the latest generation of sensitive amplifier technology, yields enough material to identify isotopic variability. Future research should employ these techniques to investigate further the presence of stratigraphic trends on various scales and isotopic disequilibrium between clinopyroxene and plagioclase. A better understanding of the variability of isotopic composition in the lower oceanic crust has implications for the location of melt emplacement and the location and extent of magma mixing at oceanic spreading centres, as well as the scale and magnitude of mantle heterogeneity.

Acknowledgements

The authors would like to thank Sergei Matveev and Jasper Berndt for their technical assistance with EMP and LA-ICPMS analyses. Chris Coath is thanked for his help with data treatment. Kathryn Goodenough, Michael Styles and David Schofield of the British Geological Survey are thanked for their help in the field. We wish to thank two anonymous reviewers and editor Cin-Ty Lee for their constructive comments that helped improve the manuscript.

Editor: Cin-Ty Lee

Additional Information

Supplementary Information accompanies this letter at http://www.geochemicalperspectivesletters.org/article1827.

Cite this letter as: Jansen, M.N., Lissenberg, C.J., Klaver, M., de Graaff, S.J., Koornneef, J.M., Smeets, R.J., MacLeod, C.J., Davies, GR.. (2018) Isotopic variation in Semail Ophiolite lower crust reveals crustal-level melt aggregation. *Geochem. Persp. Let.* 8, 37–42.

References

Bédard, J.H. (2006) Trace element partitioning in plagioclase feldspar. *Geochimica et Cosmochimica Acta* 70, 3717-3742.

Benoit, M., Polvé, M., Ceuleneer, G. (1996) Trace element and isotopic characterization of mafic cumulates in a fossil mantle diapir (Oman ophiolite). *Chemical Geology* 134, 199-214.

Cherniak, D.J. (2003) REE diffusion in feldspar. *Chemical Geology* 193, 25-41.

Coogan, L.A. (2014) The Lower Oceanic Crust. In: Holland, H.D., Turekian, K.K. (Eds.) *Treatise on Geochemistry.* Second Edition, Elsevier, Oxford, 497-541.

Coogan, L.A., O'Hara, M.J. (2015) MORB differentiation: In situ crystallization in replenished-tapped magma chambers. *Geochimica et Cosmochimica Acta* 158, 147-161.

Davidson, J.P., Tepley, F.J. (1997) Recharge in volcanic systems: evidence from isotope profiles of phenocrysts. *Science* 275, 826-829.

Godard, M., Bosch, D., Einaudi, F. (2006) A MORB source for low-Ti magmatism in the Semail ophiolite. *Chemical Geology* 234, 58-78.

De Graaff, S. (2016) *Did the Oman Ophiolite form above a subduction zone? Evidence from widespread later-stage intrusions in the Central and Southeastern Semail Ophiolite.* MSc thesis, Vrije Universiteit Amsterdam, 42 pp.

Klein, E.M., Langmuir, C.H. (1987) Global correlations of ocean ridge basalt chemistry with axial depth and crustal thickness. *Journal of Geophysical Research: Solid Earth* 92, 8089-8115.

Koga, K.T., Kelemen, P.B., Shimizu, N. (2001) Petrogenesis of the crust-mantle transition zone and the origin of lower crustal wehrlite in the Oman ophiolite. *Geochemistry, Geophysics, Geosystems* 2, 2000GC000132.

Lange, A.E., Nielsen, R.L., Tepley, F.J., Kent, A.J.R. (2013) Diverse Sr isotope signatures preserved in mid-oceanic-ridge basalt plagioclase. *Geology* 41, 279–282.

Lissenberg, C.J., MacLeod, C.J. (2016) A Reactive Porous Flow Control on Mid-ocean Ridge Magmatic Evolution. *Journal of Petrology* 57, 2195-2220.

Lissenberg, C.J., MacLeod, C.J., Howard, K.A., Godard, M. (2013) Pervasive reactive melt migration through fast-spreading lower oceanic crust (Hess Deep, equatorial Pacific Ocean). *Earth and Planetary Science Letters* 361, 436-447.

MacLeod, C.J., Yaouancq, G. (2000) A fossil melt lens in the Oman ophiolite: Implications for magma chamber processes at fast spreading ridges. *Earth and Planetary Science Letters* 176, 357-373.

MacLeod, C.J., Lissenberg, C.J., Bibby, L.E. (2013) "Moist MORB" axial magmatism in the Oman ophiolite: The evidence against a mid-ocean ridge origin. *Geology* 41, 459-462.

McCulloch, M.T., Gregory, R.T., Wasserburg, G.J., Taylor Jr, H.P. (1980) A neodymium, strontium, and oxygen isotopic study of the Cretaceous Samail ophiolite and implications for the petrogenesis and seawater-hydrothermal alteration of oceanic crust. *Earth and Planetary Science Letters* 46, 201-211.

Nicolas, A. (1989) *Structures of ophiolites and dynamics of ocean lithosphere*. Kluwer Academic Publishers, Dordrecht, 367 pp.

O'Neill, H., Jenner, F.E. (2012) The global pattern of trace-element distributions in ocean floor basalts. *Nature* 491, 698-704.

Rioux, M., Bowring, S., Kelemen, P., Gordon, S., Dudás, F., Miller, R. (2012) Rapid crustal accretion and magma assimilation in the Oman-U.A.E. ophiolite: High precision U-Pb zircon geochronology of the gabbroic crust. *Journal of Geophysical Research: Solid Earth* 117, B07201.

Rioux, M., Bowring, S., Kelemen, P., Gordon, S., Miller, R., Dudas, F. (2013) Tectonic development of the Samail ophiolite: High-precision U-Pb zircon geochronology and Sm-Nd isotopic constraints on crustal growth and emplacement. *Journal of Geophysical Research: Solid Earth* 118, 2085-2101.

Rubin, K.H., Sinton, J.M. (2007) Inferences on mid-ocean ridge thermal and magmatic structure from MORB compositions. *Earth and Planetary Science Letters* 260, 257-276.

Thomas, R. M. (2003) *Processes of lower crustal accretion beneath intermediate- to fast-spreading ocean ridges: constraints from the Wadi Abyad section of the Oman ophiolite.* PhD thesis, Cardiff University, 497 pp.

van Orman, J., Grove, T., Shimizu, N. (2001) Rare earth element diffusion in diopside: influence of temperature, pressure, and ionic radius, and an elastic model for diffusion in silicates. *Contributions to Mineralogy and Petrology* 141, 687-703.

Wendt, I., Carl, C. (1991) The statistical distribution of the mean squared weighted deviation. *Chemical Geology: Isotope Geoscience section* 86, 275-285.

Workman, R.K., Hart, S.R. (2005) Major and trace element composition of the depleted MORB mantle (DMM). *Earth and Planetary Science Letters* 231, 53-72.

Yang, S.H, Maier, W.D., Lahaye, Y., O'Brien, H. (2013) Strontium isotope disequilibrium of plagioclase in the Upper Critical Zone of the Bushveld Complex: evidence for mixing of crystal slurries. *Contributions to Mineralogy and Petrology* 166, 959-974.

Zindler, A., Hart, S.R., Frey, F.A., Jakobsson, S.P. (1979) Nd and Sr isotope ratios and rare earth element abundances in Reykjanes Peninsula basalts evidence for mantle heterogeneity beneath Iceland. *Earth and Planetary Science Letters* 45, 249-262.

Geochemical Perspectives Letters

Isotopic variation in Semail Ophiolite lower crust reveals crustal-level melt aggregation

M.N. Jansen, C.J. Lissenberg, M. Klaver, S.J. de Graaff, J.M. Koornneef, R.J. Smeets, C.J. MacLeod, G.R. Davies

Supplementary Information

The Supplementary Information includes:

- Extended Analytical Techniques and Data Treatment
- Tables S-1 to S-3
- Figures S-1 and S-2
- Supplementary Data Table (Table S-4; Excel download)
- Supplementary Information References

Extended Analytical Techniques and Data Treatment

1. Mineral major and trace element analysis

Mineral major and trace element data of OC and OG coded samples are published in MacLeod and Yaouancq (2000) and Thomas (2003). Carbon-coated polished thick-sections (200 μm) were produced from the OM samples lacking mineral data. Major element compositions were determined at the Vrije Universiteit Amsterdam with a JEOL JXA 8800M electron microprobe (EMP) at an acceleration voltage of 15 kV and a beam current of 25 nA (clinopyroxene) and 15-20 nA (plagioclase). Pyroxenes were analysed with a focused beam whereas plagioclase was analysed with a spot size of 10 μm. Analyses were matrix-corrected using the ZAF method and calibrated against natural and synthetic mineral standards. Two plagioclase and clinopyroxene grains were analysed in each sample and within each grain five spots were analysed in the core and five near the rim (distance from rim ≥10 μm). Mineral compositions were checked for mineral stoichiometry by normalising results to 8 atoms per formula units (apfu) O for plagioclase and 6 apfu O for pyroxene. Analyses were excluded if the sum of cations was <99.5 % or >100.5 % (for clinopyroxene) and <99.0 % or >101.0 % (for plagioclase) or if the sum of oxides was <98.5 % or >101.5 %.

Trace element concentrations in clinopyroxene and plagioclase (for the OM samples) were determined in situ by laser-ablation inductively-coupled plasma-mass spectrometry (LA-ICPMS) at the Institute of Mineralogy, Westfälische Wilhems Universität Münster, Germany. The ablation system consisted of a 193 nm excimer laser (Analyte G2, Photon Machines) coupled to an Element 2 (Thermo Fisher Scientific) single collector mass spectrometer. The laser was operated at an energy density of ~4 J/cm^2 and a spot size between 65 and 85 μm. A NIST 612 glass reference material was used as external calibration standard while glasses of BCR2-G and BIR1-G reference materials were used as secondary standards. The CaO concentrations determined by EMP were used as internal standard element (^{43}Ca) for quantification (average CaO concentrations in the sample were used as internal standard element where it was not possible to analyse the same grains analysed by EMP). Overall measurement time for single spot analysis was 60 s, with 20 s background and 40 s on peak signal. Raw data were processed using GLITTER software (Griffin *et al.*, 2008). Two clinopyroxene

and two plagioclase crystals were analysed for each sample, where possible the same grains that were analysed with EMP. For each grain, two spots were placed in the core and two were placed near the rim (≥10 μm). Glass reference materials BCR2-G and BIR1-G were used to monitor precision and accuracy (n = 10 and 8, respectively), in the absence of appropriate clinopyroxene and plagioclase trace element standards. Reproducibility of key trace elements was better than 10 % (2 RSD), but reproducibility of trace element ratios (*e.g.*, Sm/Nd) was better than 6 % (2 RSD) (see Table S-1). It should be noted that clinopyroxene and plagioclase from this study have trace elements compositions that are not entirely comparable to the BCR2-G and BIR1-G reference materials (basalts). However, for the purposes of this study, the Nd and Sm concentrations in clinopyroxene are of primary interest (for the age corrections, see also Section 5). These concentrations are of the same order of magnitude as in BIR1-G reference material, making it a suitable external standard.

Table S-1 Reproducibility of key trace elements and ratios (2 RSD).

	Number of analyses	Cr	Rb	Sr	La	Ce	Pr	Nd	Sm	Eu	Gd	Tb	Dy
BCR2-G	10	4.5%	2.8%	5.3%	1.4%	2.1%	2.1%	2.0%	2.9%	4.0%	2.0%	7.3%	6.2%
BIR1-G	8	3.4%	3.4%	17.2%	1.2%	4.5%	4.3%	4.6%	6.8%	9.9%	3.8%	10.2%	7.9%
	Number of analyses	**Ho**	**Er**	**Tm**	**Yb**	**Lu**	**Hf**	**Pb**	**Th**	**U**	**Sm/Nd**	**Rb/Sr**	**U/Pb**
BCR2-G	10	6.3%	6.8%	6.8%	5.7%	7.2%	3.7%	17.9%	5.4%	3.0%	5.4%	4.7%	16.0%
BIR1-G	8	9.2%	7.5%	8.9%	7.2%	7.8%	8.7%	16.2%	14.9%	22.8%	5.3%	16.7%	21.0%

2. Sample processing and micro-sampling

Selected hand samples were cut with a diamond blade saw into rock slabs of 1-2 cm thick, perpendicular to the foliation and parallel to the lineation. The surfaces of these slabs were polished and within each sample the largest, least altered and inclusion-free plagioclase and clinopyroxene crystals were selected using a binocular microscope (Fig. S-1). Energy-dispersive elemental maps of these crystals were made at Cardiff University with a Zeiss Sigma HD Analytical SEM equipped with dual 150 mm^2 EDS detectors to reveal any cryptic major element zoning (Ca, Mg and Fe for clinopyroxene; Ca and Na for plagioclase).

Individual crystals and crystal domains (cores, rims) were micro-sampled at the Vrije Universiteit using a Merchantek MicroMill that was operated in a laminar flowhood and Horico diamond coated drill bits with a diameter of ~500 μm. Similar micro-sampling techniques have been applied successfully in previous studies for Sm-Nd isotope analysis in single garnets (Pollington and Baxter, 2011) and for Rb-Sr isotope analysis in single plagioclase crystals (Charlier *et al.*, 2006). Before use, drill bits were cleaned by submerging them in 0.165 M HCl for 1 s and washing them in a Milli-Q water (Millipore B.V.) ultrasonic bath for 15 minutes. For micro-sampling single crystals, care was taken to avoid the immediate area near grain boundaries, where the effects of diffusion, melt-rock reactions and low temperature alteration are expected to be largest. Before drilling, the carbon coat was removed and the surfaces of the rock slabs were cleaned stepwise with Milli-Q water (60 s), ethanol (60 s), and 1 M acetic acid (30 s). Subsequently slabs were placed in a Milli-Q water ultrasonic bath for 10 minutes. See Table S-2 for blank levels determined for the micro-sampling procedure by placing a drop of Milli-Q water on a rock slab for 1-60 minutes. When drilling multiple crystals from the same rock slab, the slab was cleaned with Milli-Q water and ethanol before drilling the next crystal. The rock slabs were mounted onto the micromill stage and secured with wax. The stage offset calibration procedure requires a small hole to be drilled in the rock slab at a random location. To remove any (minor) contamination resulting from this procedure, the drill bit is submerged in a Milli-Q water drop for thirty seconds while it was rotating. After stage offset and drill-bit position calibrations were completed, a line path was drawn on the selected crystal to be traced by the drill. Paths were drawn to maximise the surface area drilled while avoiding inclusions and maintaining a distance of ~0.1 mm from the grain boundaries. Large grains (> 1-2 mm) that displayed core-to-rim major element zoning, core and rim samples were drilled sequentially. During micro-sampling, the drilled material was brought into suspension by placing a drop of Milli-Q water at the drilling spot. The Milli-Q water containing the drilled sample was pipetted into a pre-cleaned 7 ml PFA beaker and new drops were placed near the drill at regular time intervals during drilling. Drilling speed was set to 65 % and scan- and drill plunge speeds were kept low (20-30 μm/s) to avoid interlock failures due to the hardness of the crystals. The duration of micro-sampling, measured from the moment of placing of the Milli-Q water drop to the pipetting of the last material, varied between 10 to 70 minutes per grain for most samples. After drilling was completed, the optically determined dimensions and shape of the hole were used to estimate the volume sampled.

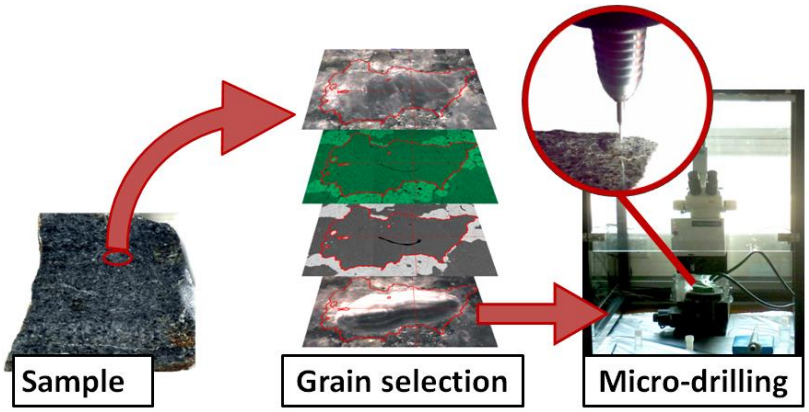

Figure S-1 Schematic workflow of the micro-sampling procedure: samples cut into rock slabs were examined under the microscope and the best-preserved grains were selected. Major element maps and backscattered electron images of the selected grains were used to identify zoning and/or inclusions. On basis of this information the crystal was sampled along a drilling pattern using a Merchantek MicroMill.

3. Sample digestion and ion-exchange chromatography

Samples recovered from the micromill were dried down and subsequently digested in PFA beakers in 1 ml of a 1:4 mixture of concentrated HNO_3 and HF on a hotplate at 140 °C for ≥48 hours. An aliquot of a ^{149}Sm-^{150}Nd mixed-spike was added to plagioclase samples prior to digestion for isotope dilution analysis of Nd and Sm concentrations. All reagents used in this study were double sub-boiling distilled to achieve low blank levels. After digestion, samples were dissolved in 0.5 ml 2.0 M HNO_3. Resins for ion-exchange chromatography were obtained from Eichrom Technologies, Inc. The light rare-earth elements (LREE) were separated from the matrix using 150 µl TRU resin columns by eluting the matrix with 3.75 ml 2.0 M HNO_3 (elution volume is including the 0.5 ml sample load) and eluting the LREE fraction with 1.5 ml Milli-Q water. For plagioclase samples, the matrix was collected and subsequently dried down, re-dissolved in 0.5 ml 3.0 M HNO_3, and loaded onto 75 µl Sr resin columns. Sr was eluted with 1.0 ml Milli-Q water following the elution of the matrix with 2.25 ml 3.0 M HNO_3. Sr isotopes in clinopyroxene are not expected to reflect the magmatic source due to high diffusion rates and sensitivity to hydrothermal alteration (Sneeringer *et al.*, 1984; Kempton and Hunter, 1997) and were therefore not considered herein. The REE fraction was dried down, re-dissolved in 0.5 ml 0.165 M HCl and loaded onto 0.75 ml Ln resin columns. After elution of the La, Ce and the bulk of Pr (9.5 ml 0.165 M HCl), Nd was eluted with 4.0 ml 0.3 M HCl, followed by Sm elution for ID samples using 5.0 ml of 0.5 M HCl. Collected Sr, Nd and Sm fractions were dried down and treated with concentrated HNO_3 prior to TIMS analysis. Total procedural blanks are listed in Table S-2 and are typically <1 % of the sample size for Nd and Sm and <1 ‰ for Sr, and thus considered to be negligible.

Table S-2 Blanks determined by isotope dilution for the micro-sampling procedure, the total cleanroom procedural blank (digestion and ion-exchange chromatography) and typical loading blanks. These values are consistent with other studies from the same laboratory (*e.g.*, Klaver, 2016). n.d. – not determined. b.d.l. – below detection limit.

		Nd (pg)	Sr (pg)	Sm (pg)
Microsampling procedure	1 min. of drilling	0.07	61	n.d.
	60 min. of drilling	b.d.l	59	n.d.
Cleanroom procedure	Plagioclase series	0.96	30.2	0.29
	Clinopyroxene series	0.59-5.81	17.0-57.7	n.d.
Loading blank		<0.01	3	n.d.

4. TIMS analyses

Isotopic analyses were performed using a Thermo Scientific Triton *Plus* thermal ionisation mass spectrometer (TIMS) at the Vrije Universiteit Amsterdam using single (Sr) and double (Nd and Sm) annealed Re filaments. Whereas sufficient Sr was available to follow regular analytical protocols (*e.g.*, Font *et al.*, 2012), low amounts of Nd (200-600 pg) and Sm (50-250 pg) in the plagioclase samples required the use of 10^{13} Ω resistors fitted in the Faraday cup amplifier feedback loop (hereafter referred to as "10^{13} Ω

amplifiers"; Koornneef *et al.*, 2014; Klaver *et al.*, 2016).

Strontium samples were loaded together with 2 µl of a $TaCl_5$ activator (concentration = 10 µg Ta/µl) to enhance ionisation. Measurements were carried out in static multi-collection mode using default 10^{11} Ω amplifiers at ^{88}Sr ion beam currents of ~4.5×10^{-12} A (equivalent to a signal intensity of 4.5 V) for 200 cycles of 8.4 s integration time with a 30 s baseline measurement every 20 cycles. Instrumental mass fractionation was corrected for by normalising to $^{88}Sr/^{86}Sr = 8.375209$ using the exponential law (Thirlwall, 1991) and data were subjected to an online 2 SD outlier test. Isobaric interference of Rb was monitored at mass 85 but was found to be negligible and hence no correction was required for interference of ^{87}Rb on ^{87}Sr. Repeated analyses of NIST SRM 987 yielded $^{87}Sr/^{86}Sr = 0.710257 \pm 34$ (2 SD; n = 11) over the course of this study. All data are reported relative to $^{87}Sr/^{86}Sr = 0.710245$ for SRM 987. Due to low Rb concentrations (<0.05 ppm; Supplementary Data Table) in plagioclase, ingrowth of ^{87}Sr after crystallisation was assumed to be negligible and hence no age correction was applied.

Neodymium and samarium samples were loaded on double filaments together with 1 µl 1% H_3PO_4. Clinopyroxene samples contained sufficient Nd (3-6 ng) for analysis with default 10^{11} Ω amplifiers whereas the low amounts of Nd and Sm in plagioclase samples necessitated the use of 10^{13} Ω amplifiers (Table S-3) to improve the signal-to-noise ratio by a theoretical factor of 10. In practice, however, an improvement of a factor ~2-3 in external precision (reproducibility) can be achieved with the use of 10^{13} Ω amplifiers (Koornneef *et al.*, 2014; Klaver *et al.*, 2016). A similar measurement strategy is followed for all Nd and Sm analyses, regardless of amplifiers used. A 660 s baseline measurement was conducted during filament warm-up to allow continuous data acquisition afterwards. Data acquisition was started at low signal intensities, directly after beam optimisation and peak centring, and samples were run to exhaustion. The signal was monitored continuously during measurement and filament currents were adjusted to keep the ion beam as stable as possible. Measurement durations varied between 16 and >200 cycles of 8.4 s integration time, with an average of 115 cycles for Nd in clinopyroxene, 270 cycles for Nd in plagioclase samples and 150 cycles for Sm in plagioclase. The use of 10^{13} Ω amplifiers necessitated an external gain calibration as online calibration using an internal reference current (0.333333 pA) was not possible. The La Jolla Nd standard was used to determine gain factors for these amplifiers following Trinquier (2014). The 10^{13} Ω amplifiers were assigned to different cups through the Triton amplifier relay board and ^{144}Nd and ^{146}Nd (the most abundant measured Nd isotopes) were measured on default, gain-corrected 10^{11} Ω amplifiers (Table S-3). This allowed correction for instrumental mass fractionation to $^{146}Nd/^{144}Nd = 0.721903$. Any residual offset between measured $^{143}Nd/^{144}Nd$, $^{145}Nd/^{144}Nd$, $^{148}Nd/^{144}Nd$ and $^{150}Nd/^{144}Nd$ and the long-term average was then ascribed to variations in amplifier gain. Gain factors were calculated in this way on a daily basis and entered in the amplifier system table of the Triton software such that gain corrections were performed automatically online. All measurements were then corrected offline for a 3-month average of the gain factors (September – November 2015, during which analyses in this study were performed; n = 27). The robustness of gain factors calculated in such a way was shown by Klaver *et al.* (2016) and any residual scatter introduced by this method is accounted for by incorporating the reproducibility of secondary standards measured at the same conditions in the quoted measurement uncertainties (see below).

Data reduction was performed offline to allow deconvolution of the spike contribution in the isotope-dilution runs. Clinopyroxene data were filtered to include only ratios measured at ^{143}Nd currents of ≥1.0 pA (equivalent to 100 mV signal intensity on a default 10^{11} Ω amplifier) where possible, but for two samples data acquired at lower currents were included (sample 95OG16-cpx-core at ≥0.3 pA; sample 95OC41-cpx at ≥0.5 pA; equivalent to 30 and 50 mV on a default 10^{11} Ω amplifier, respectively). For clinopyroxene samples, no further outliers were removed unless they were conspicuously related to signal instability. Plagioclase data were filtered to include only ratios measured at ^{143}Nd currents of ≥0.05 pA (equivalent to 5 mV signal intensity on a default 10^{11} Ω amplifier) and subsequently subjected to a 2 SD outlier test. Isobaric interference of Sm on ^{144}Nd and ^{150}Nd was monitored at mass ^{147}Sm. Two samples (14OM4-plg-id3 and 14OM5-plg-id) showed minor Sm interference ($^{147}Sm/^{144}Nd$ <0.0005) during the Nd measurement, which was corrected by calculating the Sm composition (mass 144 and 150) of the spike-sample mix and subtracting that from the raw ^{144}Nd and ^{150}Nd data, respectively. Only Sm isotopes free from Nd interference were used in the data reduction and Gd was quantitatively removed during chemical separation, hence no interference correction was required (Table S-3). The raw data were corrected for instrumental mass fractionation and spike contribution following the iterative approach described by Stracke *et al.* (2014) and by normalising to $^{146}Nd/^{144}Nd = 0.721903$ and $^{147}Sm/^{152}Sm = 0.56081$ (Carlson *et al.*, 2007) on a cycle-by-cycle basis. Resultant average $^{150}Nd/^{144}Nd$ and $^{149}Sm/^{152}Sm$ were used to calculate Nd and Sm concentrations following standard isotope dilution equations. This spike-stripping approach has been demonstrated to yield accurate and precise $^{143}Nd/^{144}Nd$ data even at high spike-sample ratios (Stracke *et al.*, 2014). Nevertheless, samples were underspiked by a factor 10-20 to mitigate any potential effect of spike contribution on the isotope composition, which resulted in only a marginal increase in error magnification for Sm and Nd concentrations. The uncertainty on Sm/Nd as determined by isotope dilution is estimated from the long-term reproducibility of USGS reference materials BHVO-2 and BCR-2 (measured on regular sample sizes) to be better than 0.5 %.

Table S-3 Cup configuration and use of detectors for Nd and Sm measurements. Interfering elements are shown in italics. Notes: *isotope used for instrumental mass fractionation correction to determine gain factors for the 10^{13} Ω amplifiers; ‡isotope used for isotope dilution data reduction, note that these isotopes suffer no Nd interference and are hence not influenced by the presence of small amounts of Nd.

Faraday cup	L3	L2	L1	axial	H1	H2	H3	H4
Nd	^{143}Nd	^{144}Nd	^{145}Nd	^{146}Nd	*^{147}Sm*	^{148}Nd	-	^{150}Nd
Interference (abundance %)		*^{144}Sm (3.1)*				*^{148}Sm (11.2)*		*^{150}Sm (7.4)*
Clinopyroxene	10^{11} Ω	10^{11} Ω	10^{11} Ω	10^{11} Ω	10^{11} Ω	10^{11} Ω	-	10^{11} Ω
Plagioclase	**10^{13} Ω**	**10^{13} Ω**	10^{11} Ω	**10^{13} Ω**	10^{11} Ω	10^{11} Ω	-	**10^{13} Ω**
Gain calibration	**10^{13} Ω**	**10^{11} Ω***	**10^{13} Ω**	**10^{11} Ω***	10^{11} Ω	**10^{13} Ω**	-	**10^{13} Ω**
Sm	*^{146}Nd*	^{147}Sm‡	^{148}Sm	^{149}Sm‡	^{150}Sm	^{152}Sm‡	-	-
Interference (abundance %)			*^{148}Nd (5.7)*		*^{150}Nd (5.6)*	*^{152}Gd (0.2)*		
Plagioclase	10^{11} Ω	**10^{13} Ω**	**10^{13} Ω**	**10^{13} Ω**	10^{11} Ω	**10^{13} Ω**	-	-

5. Data quality and treatment of uncertainties

In the absence of obvious temporal drift in gain factors, the 3-month average gain factors were used to recalculate all raw data offline. Reproducibility of ^{143}Nd/^{144}Nd for standards measured with 10^{13} Ω amplifiers after gain calibration was 148 ppm (2 RSD) for artificial standard CIGO (mean = 0.511373 ± 0.000076; n = 23; various amounts ranging 0.3-250 ng Nd) and 161 ppm for BCR-2 reference material (mean = 0.512644 ± 0.000082; n = 11; 0.15-0.34 ng Nd) (Fig. S-2, Table S-4f). Repeated analyses of ^{143}Nd/^{144}Nd for standards measured with regular 10^{11} Ω amplifiers were reproducible at 82 ppm for BCR-2 reference material (mean = 0.512630 ± 0.000042; n = 12; 1.9-2.6 ng Nd) and 73 ppm for BHVO-2 reference material (mean = 0.512972 ± 0.000038; n = 12; 1.6-2.1 ng Nd). Standards were measured at similar signal intensities and measurement durations as samples.

The reproducibility of ^{143}Nd/^{144}Nd of samples was determined through repeated analyses of BCR-2 reference material (Fig. S-2, Table S-4f). The BCR-2 aliquots were chosen to match the size of clinopyroxene samples (2.5 ng, n = 12) and plagioclase samples (0.15-0.35 ng, n = 11), respectively, and processed using the same procedures as the samples. The reproducibility of BCR-2 was then assessed using the mean square weighted deviation (MSWD), a statistic commonly used for determining the significance of isochrons (Eqs. S-1 and S-2; Wendt and Carl, 1991). A MSWD value of 1 implies that the data fit perfectly to a homogenous composition and that the amount of scatter is in agreement with predictions based on the analytical uncertainties. The MSWD of the two sets of BCR-2 aliquots was found to be greater than 1 (Fig. S-2, centre panels), indicating that the internal precision of the individual measurements cannot account for the full variation in ^{143}Nd/^{144}Nd. The excess variance, here named x^2, appears to be intrinsic to the measurement of small samples and is, amongst others, related to the fluctuation of the 10^{13} Ω amplifier gain values during an analytical session. The true reproducibility can therefore be expressed as the quadratic sum of the measurement uncertainty and the excess variance x (Eq. S-3).

$$Weighted\ Mean = \frac{\sum \frac{1}{\sigma_i^2} \times obs_i}{\sum \frac{1}{\sigma_i^2}} \qquad \text{Eq. S-1}$$

$$MSWD = \frac{\sum \left(\frac{obs_i - weighted\ mean}{\sigma_i} \right)^2}{f} \qquad \text{Eq. S-2}$$

$$Full\ error\ of\ measurement = \sqrt{standard\ error\ of\ measurement^2 + x^2} \qquad \text{Eq. S-3}$$

where obs_i is the ^{143}Nd/^{144}Nd ratio of measurement i, σ_i is the uncertainty of measurement i, f is the degrees of freedom (in the case of this study f = n – 1), and x^2 is the excess variance.

Since the BCR-2 aliquots represent a homogeneous population, their MSWD value should equal 1 and based on this assumption the excess variance x^2 can be easily calculated in a process of iteration by solving Equations S-2 and S-3 until MSWD = 1. The resulting x^2 was found to be 0.000065 for plagioclase sample sizes and 0.000034 for clinopyroxene sample sizes (2 SD). Although the excess

variance is expected to be constant regardless of sample size, the gain calibration procedure for the 10^{13} Ω amplifiers on the TIMS is known to introduce residual scatter in the measurements (Klaver, 2016) and probably affected the plagioclase analyses. Fully propagated uncertainties for Nd isotope measurements on samples were obtained with Equation S-3 using the measurement standard error and the corresponding excess variance.

Plagioclase $^{143}Nd/^{144}Nd$ ratios were age corrected (96 Ma) using the Sm/Nd ratios obtained from ID-TIMS and the corresponding uncertainties were propagated. For clinopyroxene samples the average Sm and Nd concentrations from LA-ICPMS spots on the thick-sections were used (*i.e.* from crystals coexisting in the same hand sample). Sm/Nd ratios in clinopyroxene ranged from 0.38 and 0.8 and the typical variability of Sm/Nd in one hand sample was between 0.05 and 0.2, which corresponds to a variability between 0.000019 and 0.000076 in the initial $^{143}Nd/^{144}Nd$. Most of the cited Sm/Nd variability, however, occurs within individual grains rather than between grains within a hand sample, thus justifying the average Sm/Nd ratio of coexisting grains as a reasonable estimate for the purpose of age corrections. The uncertainty on the Sm/Nd ratio (Table S-1) was propagated in the age correction calculations.

To quantify the variability in Nd isotopes in the plagioclase and clinopyroxene samples, the MSWD value was calculated using the fully propagated uncertainties, which was then compared to a critical MSWD value to evaluate the significance of the deviation from 1 (homogeneity). The critical value is based on the criteria Wendt and Carl (1991) give for rejecting the hypothesis that the set of measurements represent an isochron:

$$MSWD > 1 + 2\sqrt{\frac{2}{f}} \qquad \text{Eq. S-4}$$

where f is the degrees of freedom (n – 1). This equation is derived from the variance of the theoretical MSWD frequency distribution and represents the upper limit of a 2σ confidence interval (Wendt and Carl, 1991). We note that the critical value (*i.e.* the right side of Eq. S-4) is dependent on the total number of analyses (n).

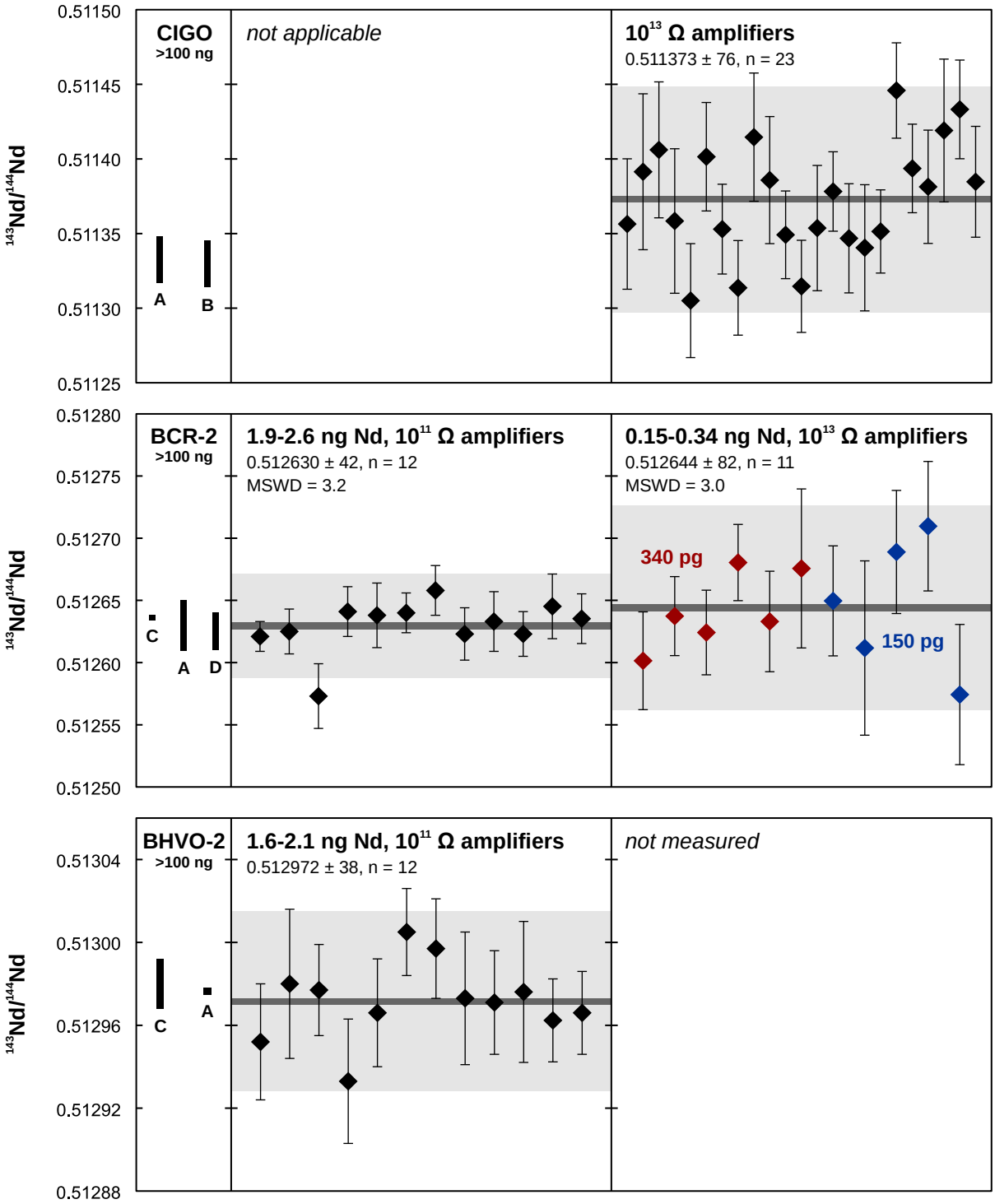

Figure S-2 Nd isotope data for reference materials measured over the course of this study. CIGO is the Vrije Universiteit in-house Nd standard made from Nd_2O_3 powder; the reference value is 0.511342, which relates to La Jolla = 0.511852 (Griselin *et al.*, 2001). Aliquots of USGS standards BHVO-2 and BCR-2 at the same size as samples (~2 ng Nd for clinopyroxene, ~0.3 ng Nd for plagioclase) were measured to assess the reproducibility of the method. These data points reflect aliquots of standard that were processed individually through the chemical separation process. The MSWD was calculated using internal precisions only and values greater than 1 indicate an (analytically related) excess variance, as discussed in the text. Notes: A – 2011-2015 average from Klaver (2016) (n = 39 for CIGO, n = 9 for BCR-2, n = 4 for BHVO-2); B – average of large (>200 ng) CIGO standards measured over the course of this study (0.511329 ± 0.000016, n = 29); C – preferred value from the GeoReM database (Jochum *et al.*, 2005); D – result for spike-stripped, ~200 ng Nd BCR-2 that was spiked for isotope dilution analysis. All error bars are 2 SE (internal precision). Grey field and bar indicate average and 2 SD. All quoted uncertainties are 2 SD.

Supplementary Data Table (Table S-4)

The Supplementary data table (Table S-4) is available for download as an Excel file at http://www.geochemicalperspectivesletters.org/article1827.

Table S-4 Supplementary data table. **(a)** EMP major element analyses of clinopyroxene. **(b)** EMP major element analyses of plagioclase. **(c)** LA-ICPMS trace element analyses of clinopyroxene. **(d)** LA-ICPMS trace element analyses of plagioclase. **(e)** TIMS neodymium and strontium isotope analyses of plagioclase and clinopyroxene crystals. **(f)** TIMS neodymium isotope analyses of reference material.

Supplementary Information References

Carlson, R.W., Boyet, M., Horan, M. (2007) Chondrite barium, neodymium, and samarium isotopic heterogeneity and early earth differentiation. *Science* 316, 1175-1178.

Charlier, B.L.A., Ginibre, C., Morgan, D., Nowell, G.M., Pearson, D.G., Davidson, J.P., Ottley, C.J. (2006) Methods for the microsampling and high-precision analysis of strontium and rubidium isotopes at single crystal scale for petrological and geochronological applications. *Chemical Geology* 232, 114-133.

Font, L., van der Peijl, G., van Wetten, I., Vroon, P., van der Wagt, B., Davies, G. (2012) Strontium and lead isotope ratios in human hair: investigating a potential tool for determining recent human geographical movements. *Journal of Analytical Atomic Spectrometry* 27, 719-732.

Griffin, W., Powell, W., Pearson, N., O'Reilly, S. (2008) GLITTER: data reduction software for laser ablation ICP-MS. Laser Ablation-ICP-MS in the Earth Sciences. *Mineralogical Association of Canada Short Course Series* 40, 204-207.

Griselin, M., Van Belle, J., Pomies, C., Vroon, P., Van Soest, M., Davies, G. (2001) An improved chromatographic separation technique of Nd with application to NdO+ isotope analysis. *Chemical Geology* 172, 347-359.

Jochum, K.P., Nohl, U., Herwig, K., Lammel, E., Stoll, B., Hofmann, A.W. (2005) GeoReM: a new geochemical database for reference materials and isotopic standards. *Geostandards and Geoanalytical Research* 29, 333-338.

Kempton, P.D., Hunter, A.G. (1997) A Sr-, Nd-, Pb-, O-isotope study of plutonic rocks from MARK, Leg 153: implications for mantle heterogeneity and magma chamber processes, *Proceedings of the Oceanic Drilling Program Scientific Results* 153, 305-319.

Klaver, M. (2016*) Dynamics of magma generation and differentiation in the central-eastern Aegean arc*. PhD thesis, Vrije Universiteit, Amsterdam.

Klaver, M., Smeets, R., Koornneef, J.M., Davies, G., Vroon, P. (2016) Pb isotope analysis of ng size samples by TIMS equipped with a 10^{13} Ω resistor using a ^{207}Pb-^{204}Pb double spike *Journal of Analytical Atomic Spectrometry* 31, 171-178.

Koornneef, J., Bouman, C., Schwieters, J., Davies, G. (2014) Measurement of small ion beams by thermal ionisation mass spectrometry using new 10^{13} Ohm resistors. *Analytica Chimica Acta* 819, 49-55.

MacLeod, C.J., Yaouancq, G. (2000) A fossil melt lens in the Oman ophiolite: Implications for magma chamber processes at fast spreading ridges. *Earth and Planetary Science Letters* 176, 357-373.

Pollington, A.D., Baxter, E.F. (2011) High precision microsampling and preparation of zoned garnet porphyroblasts for Sm–Nd geochronology. *Chemical Geology* 281, 270-282.

Sneeringer, M., Hart, S.R., Shimizu, N. (1984) Strontium and samarium diffusion in diopside. *Geochimica et Cosmochimica Acta* 48, 1589-1608.

Stracke, A., Scherer, E.E., Reynolds, B.C. (2014) Application of Isotope Dilution in Geochemistry. In: Holland, H.H., Turekian, K.K. (Eds.) *Treatise on Geochemistry.* Second Edition, Elsevier, Oxford, 71-86.

Thirlwall, M. (1991) Long-term reproducibility of multicollector Sr and Nd isotope ratio analysis. *Chemical Geology: Isotope Geoscience section* 94, 85-104.

Thomas, R. M. (2003) *Processes of lower crustal accretion beneath intermediate- to fast-spreading ocean ridges: constraints from the Wadi Abyad section of the Oman ophiolite.* PhD thesis, Cardiff University.

Trinquier, A. (2014) Gain calibration protocol for 10^{13} Ω resistor current amplifiers using the certified neodymium standard JNdi-1 on the TRITON *Plus*. *Thermo Fischer Scientific Technical Note* 30285.

Wendt, I., Carl, C. (1991) The statistical distribution of the mean squared weighted deviation. *Chemical Geology: Isotope Geoscience section* 86, 275-285.